



Removal of arsenic from aqueous solutions using MgFe_2O_4 nano spinel and $\text{GO}/\text{MgFe}_2\text{O}_4$ nanocomposite: an application of response surface methodology

Seyed Ali Hosseini*, Ozra Gholipoor

Department of Applied Chemistry, Faculty of Chemistry, Urmia University, Urmia, Iran, emails: s_ali_hosseini@yahoo.com, a.hosseini@urmia.ac.ir (S.A. Hosseini), ozragholipoor@yahoo.com (O. Gholipoor)

Received 15 January 2017; Accepted 22 August 2017

ABSTRACT

The adsorptive performance of MgFe_2O_4 nanoparticles and graphene oxide (GO)/ MgFe_2O_4 nanocomposite was investigated in the removal of arsenic from aqueous solutions. The statistical study of the adsorption process was carried out by response surface methodology. Experimental factors such as sample pH, contact time (min), arsenic concentration (ppm) and adsorbent dosage (g) were considered for the optimization of the adsorption process. Under the optimum conditions, the values of initial arsenic concentration, contact time, pH and adsorbent dosage were 41 ppm, 30 min, 7.16 and 0.03 g, respectively. The removal of arsenic under optimum conditions was predicted 99% and resulted in 97% in practice. The Pareto analysis suggested that order of relative importance of the factors is as follows: adsorbent dosage > pH > contact time > arsenic concentration. $\text{GO}/\text{MgFe}_2\text{O}_4$ nanocomposite showed a higher capacity than GO for adsorption of arsenic.

Keywords: Adsorption; Graphene oxide; MgFe_2O_4 nano spinel; Arsenic removal; Response surface methodology

1. Introduction

A group of metals and metalloids that have a density greater than 5 g cm^{-3} and atomic weights ranging from 63.5 to 200.6 are called heavy metals [1]. Both natural and anthropogenic activities have greatly contributed to heavy metal release in the environment and natural water system through metal plating, pesticides, metallurgical, mining, fossil fuel, tannery and production of different plastics [2,3]. The toxic effects of heavy metals on human health have been investigated extensively; they represent serious threats to the human health and water pollution [4]. Some of the toxic heavy metals that can be harmful to human body include cadmium, lead, arsenic and mercury. Though the human body needs a small dose of some heavy metals such as manganese, iron, chromium, copper and zinc because they are basic essential micronutrients; however, the presence of large quantities of these metals

may be extremely dangerous [1,5]. Due to the toxicity of most heavy metals, removal of these toxic ions from wastewater is necessary for the human health. Several techniques like reverse osmosis, coagulation, oxidation, membrane filtration, ion-exchange and adsorption. Using alternative inexpensive materials as potential sorbents to removal heavy metals have been emphasized recently [6,7].

Arsenic contamination in groundwater is increasingly causing serious concerns globally due to its toxicity and carcinogenicity; arsenic is causing serious environmental problems for healthy humans and other living organisms through arsenic-contaminated drinking water [8–10]. Arsenic exists in the environment in both inorganic and organic forms. Arsenic combined with elements like oxygen, chlorine and sulfur are called inorganic arsenic and arsenic combined with carbon and hydrogen are called organic arsenic, but in natural waters, the most common inorganic arsenic species include As(III) and As(V) [11–13]. Arsenic toxicity is dependent on its oxidation, solubility and its various forms [14]. Aqueous solutions of inorganic arsenic compounds are more toxic

* Corresponding author.

than organic arsenic to humans [15]. Arsenic exists in several oxidation states such as +5 (arsenate), +3 (arsenite), 0 (arsenic) and –3 (arsine) in aquatic systems [16]. Long-term exposure to arsenic-contaminated water with concentrations equal to or greater than 50 ppb can lead to various health problems such as skin lesions, several types of cancer in organs such as skin, lungs, liver, bladder, kidney, diabetes mellitus, adverse reproductive outcomes, gastrointestinal disease, bone marrow disorder, cardiovascular disease and other diseases. Due to the high toxicity of arsenic in drinking water to abate health problems associated with arsenic in drinking water [8,17,18]. In 1993, the World Health Organization (WHO) has reduced the previous standard of 50 ppb to a new arsenic standard of 10 ppb maximum permissible arsenic in drinking water [12,19]. The economic method to remove arsenic and other metals from aqueous solutions is adsorption and there are some many reports in literature for the removal of arsenic using different adsorbents [20–23]. Spinel-type mixed oxides could be alternative adsorbents for the removal of arsenic. Normal spinel oxides have the AB_2O_4 formula, where A atoms (divalent cations) occupy tetrahedral voids and B (trivalent cations) occupy octahedral voids. For the inverse spinel structure atoms A (divalent cations) and half the B (trivalent cations) occupy octahedral voids and half the B (trivalent cations) occupy tetrahedral voids [24–26].

Spinel ferrite nanoparticles are a kind of soft magnetic spinels with the general formula MFe_2O_4 , where M is a divalent metal ion (e.g., Ni, Mn, Mg, Zn, Co and Cu) have been extensively employed in technical applications such as in photoelectric devices, gas sensors, water splitting, microwave devices, magnetic pigment, nanodevices and catalytic properties [27–29]. Various techniques have been developed to prepare ferrite spinel such as coprecipitation, sol–gel, microemulsion, ultrasonic cavitation approach, hydrothermal and microwave synthesis [30,31].

Recently, the uses of nanosized ferrite materials have been reported for the treatment of wastewater due to their specific characteristics such as thermal stability, their reduced obtaining cost, high surface area, easy recovery using their magnetic properties, etc [32,33]. Among different ferrites, magnesium ferrite ($MgFe_2O_4$) finds application in microwave devices, as gas and humidity sensor, as semiconductor and high-density recording media. Though $MgFe_2O_4$ has been proved as a good adsorbent for dyes and different metals but the adsorbent efficiency of $MgFe_2O_4$ for As(III) has not yet been investigated [34–38]. Hence, the adsorption study of As(III) by $MgFe_2O_4$ was our interest that we did and reported in this paper.

On another hand, the study of the adsorptive removal of As(III) by the minimum experiments and saving the time and cost was important. A logic way to get it is using of experimental design methods. Response surface methodology (RSM) is an important technique for experimental design and analyzing effects of several independent variables and thus searching optimum conditions for desirable responses and to optimize the processes or products. These techniques are nowadays widely employed for the optimization of a number of processes including adsorption studies and have been successfully applied for metal removal [39].

The aims of this research were to synthesize and to study the adsorptive performance of $MgFe_2O_4$ in the removal of As(III) from wastewater. In order to save the study time and costs, the minimum number of experiments was designed by RSM. A mathematical model was developed and the optimum conditions were predicted. The effects of various parameters such as the adsorbent dosage, pH, contact time and arsenic concentration were investigated thoroughly to evaluate optimum conditions. Furthermore, the adsorptive performance of $GO/MgFe_2O_4$ was investigated for the removal of As(III) from the aqueous solution. The adsorbents were characterized by X-ray diffraction (XRD), Fourier transform infrared spectroscopy (FTIR) and scanning electron microscopy (SEM).

2. Experimental

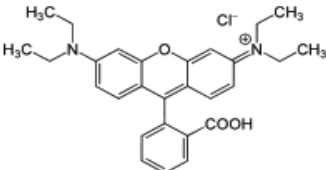
2.1. Materials

All solutions were prepared using analytical reagent grade chemicals unless otherwise specified and doubly distilled deionized water. As_2O_3 was supplied from the Sigma (USA). KIO_3 , NaOH, HCl, CH_3COOH , $C_2H_3O_2NH_4$, NH_3 , $Mg(NO_3)_2 \cdot 6H_2O$, $Fe(NO_3)_3 \cdot 9H_2O$ and Rhodamine B were purchased from the Merck (Germany). The chemical structure and characteristics of Rhodamine B are presented in Table 1.

2.2. Spectrophotometric method

Standard As(III) stock solution (1 mg mL^{-1}) was prepared by dissolving 13.2 mg of As_2O_3 in 100 mL distilled water. Working standard solution As(III) was prepared by appropriate dilution of stock solution. 0.05% solution of Rhodamine B was prepared by dissolving 2.5 mg of Rhodamine B in the volumetric flask of 100 mL distilled water stored in ambered color bottle. Potassium iodate, 1%, aqueous solution; hydrochloric acid, 0.4 M aqueous solution, acetate buffer (pH 4.5) was prepared by dissolving 774 mg of ammonium acetate in 50 mL water. Solution pH was adjusted to 4.5 with acetic acid.

Table 1
Chemical structure and characteristics of Rhodamine B

Chemical structure	Molecular formula	Molecular weight (g mol^{-1})	Chemistry class	λ_{max} (nm)
	$C_{28}H_{31}ClN_2O_3$	479.02	Cationic	555

2.3. Preparation of MgFe₂O₄

MgFe₂O₄ adsorbent nanoparticles were synthesized by a coprecipitation method. The preparation of MgFe₂O₄ was performed as follows: ammonia solution was mixed with deionized water in desired proportions until pH reached 9.2. Some Mg(NO₃)₂·6H₂O and Fe(NO₃)₃·9H₂O salts with a molar ratio of 1:2 were dissolved in deionized water and added drop by drop to a flask. The reaction was conducted under vigorous magnetic stirring to obtain the powder suspension the reaction was continued for 6 h and the precipitate was filtered, washed with deionized water and dried in a muffle furnace at 110°C for 2 h, then calcined at 600°C for 4 h.

2.4. Preparation of graphene oxide

The graphene oxide (GO) was prepared from graphite powder by a modified Hummers method. 1 g graphite powder was mixed with 20 mL of sulfuric acid (H₂SO₄). The mixture was kept at room temperature for 1 h and then was stirred vigorously for 1 h within an ice bath. Then, 0.5 g of NaNO₃ and 3 g of KMnO₄ were added gradually and the resulted suspension was stirred for 2 h in an ice bath. Afterward, it was removed from the ice bath and was stirred 2 h at the room temperature; subsequently, 50 mL deionized water was added. After 15 min, 140 mL deionized water was added. Next, the sample was stirred further at 89°C for 2 h. After that it was cooled to the room temperature followed by dropwise addition of 3 mL H₂O₂ until the color of the solution turned from dark brown to yellow. The solid product was separated by centrifugation and washed several times with distilled water until the pH of the solution became neutral. The residue was dried at 60°C overnight. A suspension solution with a concentration of 1 ppm was prepared and placed for 20 min in the ultrasonic bath and finally, it was dried in an electric oven.

2.5. Preparation of GO/MgFe₂O₄

Some GO and MgFe₂O₄ salts with a molar ratio of 1:1 were dissolved in 20 mL ethanol and kept under ultrasonication for 40 min. The collected precipitate was filtered, washed with deionized water and dried in a muffle furnace at 110°C for 2 h.

2.6. Characterization of the nanocomposite

The structure and crystal phase of catalyst were investigated by a Philips PW1800 diffractometer and Cu K_α radiation (λ = 1.54 Å).

The FTIR spectra of the sample were recorded in transmittance at room temperature using a Bruker spectrometer (model TENSOR 27) in the range 400–4,000 cm⁻¹.

The morphology of the mixed oxides was determined via SEM by a Philips XL30 instrument with precoating samples with gold.

2.7. Determination of p*H*_{pzc} of the adsorbents

The point of zero charges (p*H*_{pzc} values) is the point at which the net charge on the adsorbent surface is zero. The p*H*_{pzc} values of MgFe₂O₄ and GO/MgFe₂O₄ were determined by pH drift method [39]. Briefly, several solutions containing

0.01 M NaCl were supplied. The initial pH (p*H*_i) of the solutions was adjusted to a value between 2 and 11 using 0.1 M HCl or 0.1 M NaOH. 0.02 g adsorbent was added to the solution. The electrolyte solution with a certain amount of an adsorbent was equilibrated for 24 h. After equilibrium, the final pH (p*H*_f) was recorded. The p*H*_f was plotted against the initial pH (p*H*_i) values. The pH at which p*H*_f crossover the (p*H*_i) was referred to as the p*H*_{pzc}.

2.8. Adsorption experiments

Standard As(III) stock solution (100 mg mL⁻¹) was prepared by dissolving 13.2 mg of As₂O₃ in 100 mL distilled water. Different concentrations of arsenic were obtained by diluting the main solution. Experiments were performed according to RSM design matrix given in Table 2. The range of pH, contact time, arsenic concentration and adsorbent dosage were 4–8, 40–60 min, 20–40 ppm and 0.4–0.8 g, respectively. Arsenic concentration was determined using UV–Vis spectrophotometer (PG Instrument 80+) at λ_{max} = 554 nm. The response (As(III) removal percentage) was expressed as percentage of As(III) removal calculated by Eq. (1):

$$\text{Removal\%} = \frac{C_0 - C}{C_0} \times 100 \quad (1)$$

where C₀ and C are the initial and final arsenic concentrations (ppm), respectively.

2.9. Experimental design, statistical analysis and optimization by RSM

In order to develop a model for the adsorption process for predicting the removal percentage of As(III) under untested conditions, we considered most important factors: initial arsenic concentration (X₁), adsorbent dosage (X₂), contact time (X₃) and pH (X₄) to investigate their effects on arsenic removal. 31 experiments were designed and optimized based on the central composite method of RSM. Each experiment was tested twice and the average of response was considered. The removal percentage for each experiment was reported with a precision of ±1%. The following second-order polynomial response model (Eq. (2)) was used to explain the behavior of the system:

$$Y = b_0 + \sum_{i=1}^n b_i X_i + \sum_{i=1}^n b_{ii} X_i^2 + \sum_{i=1}^{n-1} \sum_{j=i+1}^n b_{ij} X_i X_j \quad (2)$$

where Y is the arsenic removal, X_i and X_j are coded factors that influence the response Y (terms of the model), and B₀ is the constant term, B_i is the *i*th linear coefficient, B_{ii} is the *i*th quadratic coefficient and B_{ij} is the *ij*th interaction effect. Results were interpreted by the analysis of variance (ANOVA) using Minitab 17 software.

3. Results and discussion

3.1. Characterization of the adsorbents

The FTIR spectra of GO, MgFe₂O₄ and GO/MgFe₂O₄ are shown in Fig. 1. In the spectrum of GO, the peaks at

Table 2
RSM design matrix and the values response

Run	pH	Time (min)	Concentration (ppm)	Adsorbent dosage (g)	Experimental values (%)	Predicted values (%)
1	8	60	20	0.4	81.25	81.19
2	6	50	30	0.6	93.00	92.57
3	4	60	40	0.4	86.50	85.56
4	2	50	30	0.6	92.00	92.46
5	6	70	30	0.6	74.00	75.25
6	6	50	10	0.6	91.00	89.84
7	8	60	40	0.8	80.00	77.46
8	8	40	40	0.4	93.75	92.98
9	8	60	20	0.8	90.00	90.80
10	4	40	40	0.4	93.75	93.06
11	4	40	20	0.8	88.00	88.13
12	6	30	30	0.6	81.00	80.75
13	4	60	40	0.8	84.00	84.05
14	6	50	30	0.6	93.00	92.57
15	6	50	30	0.6	93.00	92.57
16	4	40	40	0.8	93.75	92.67
17	6	50	30	0.2	83.00	83.22
18	6	50	30	0.6	92.00	92.57
19	8	40	40	0.8	92.00	92.59
20	6	50	50	0.6	90.00	92.17
21	10	50	30	0.6	86.00	86.54
22	4	40	20	0.4	76.00	77.39
23	4	60	20	0.8	97.00	96.63
24	6	50	30	0.6	93.00	92.57
25	8	60	40	0.4	79.00	78.98
26	6	50	30	0.6	92.00	92.57
27	6	50	30	1.0	91.66	92.44
28	4	60	20	0.4	87.50	87.02
29	8	40	20	0.8	89.00	88.80
30	6	50	30	0.6	92.00	92.57
31	8	40	20	0.4	78.00	78.06

1,050.50 are assigned to the C–O stretching vibration. The peaks at 1,580.28 and 3,396.18 cm^{-1} correspond to the stretching vibrations of C=O and hydroxyl groups, respectively.

The FTIR spectrum of MgFe_2O_4 particles was also recorded for better illustration of surface groups. The presence of absorption peaks at 541.15 and 454.62 cm^{-1} confirms the formation of MgFe_2O_4 with cubic spinel structure. The absorption peak at about 541.15 cm^{-1} can be attributed to the stretching vibration of the tetragonal groups of ($\text{Fe}^{3+}\text{O}^{2-}$ or $\text{Mg}^{2+}\text{O}^{2-}$) bond. The band at 454.62 cm^{-1} is due to the vibration modes of octahedral groups ($\text{Fe}^{3+}\text{O}^{2-}$).

The FTIR spectrum of the GO/ MgFe_2O_4 shows all the peaks appeared at the spectra of MgFe_2O_4 and GO, just the intensity of peaks has been relatively low.

It is seen from Fig. 2 that the XRD pattern consists of well-resolved peaks, which confirms the polycrystalline of the prepared material. The diffraction peaks corresponding to planes (220), (311), (222), (400), (422), (333), (440) and (620)

provide a clear evidence for the formation of spinel structure of the ferrite matches well with JCPDS (73-2410) file for MgFe_2O_4 [11]. This observation matches well with those of earlier reporters [32,33]. It is also noted that the ferrite concludes some residual $\alpha\text{-Fe}_2\text{O}_3$ phase. The grain size of MgFe_2O_4 is obtained using Scherrer's formula (Eq. (3)) as 35 nm.

$$D = \frac{0.89\lambda}{\beta \cos\theta} \quad (3)$$

The morphology and particle size of MgFe_2O_4 and GO/ MgFe_2O_4 are shown in Fig. 3. It is observed in Fig. 3(a) that the MgFe_2O_4 particles are as spherical granules, whereas, in the case of GO/ MgFe_2O_4 (Fig. 3(b)), these granules are spread on the GO sheets. The average particle size of MgFe_2O_4 particles is small than 100 nm, indicating that the particles are nanoscale.

3.2. Results of response surface methodology

Based on the results of RSM, an empirical relationship between the response and independent variables was determined as the following second-order polynomial Eq. (4):

$$Y = 92.571 + 0.583X_1 + 2.305X_2 - 1.375X_3 - 1.479X_4 - 0.391X_1^2 - 1.183X_2^2 - 3.641X_3^2 - 0.766X_4^2 - 2.781X_1X_2 - 4.281X_1X_3 - 1.625X_3X_4 \quad (4)$$

According to the equation, the singular terms containing X_1 and X_2 have a positive sign, indicating a synergistic effect on the response, whereas the singular terms containing

X_3 and X_4 with a negative sign have an antagonistic effect on the response, meaning that an increase in time and pH decreases the removal percentage of arsenic. Among singular term, the X_1 (arsenic concentration) with the smallest coefficient has the minimum impact on the response (arsenic removal). Among binary terms, the interactions of X_1X_2 , X_1X_3 and X_3X_4 have a negative effect on the response.

The results of ANOVA for the model are presented in Table 3. The ANOVA suggests whether the equation is adequate to describe the relationship between the response and the significant variables [39].

The Fisher's F test was used to verify the statistical significance of the model and approved the significance of the model with F value of 74.59. The significance of the model was evaluated by the correlation coefficient (R^2), which is a

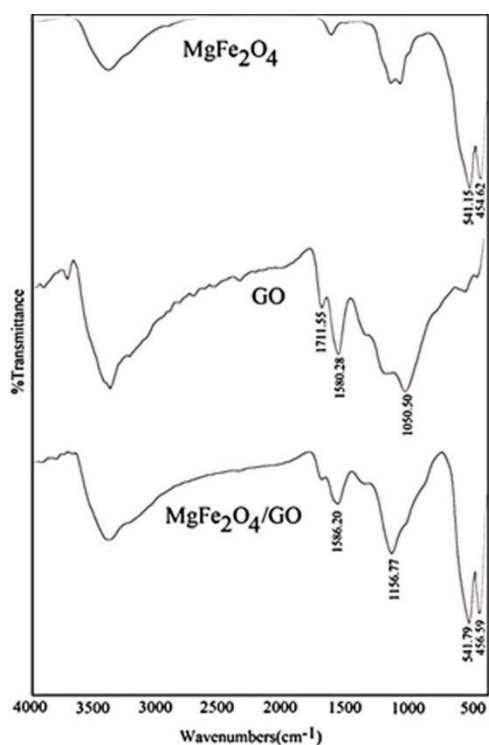


Fig. 1. FTIR spectra of $MgFe_2O_4$, GO and $GO/MgFe_2O_4$.

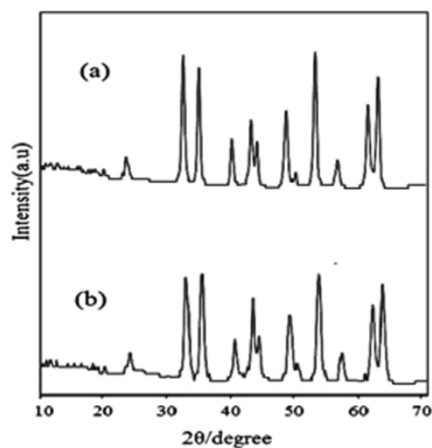


Fig. 2. The XRD patterns of (a) $MgFe_2O_4$ and (b) $GO/MgFe_2O_4$.

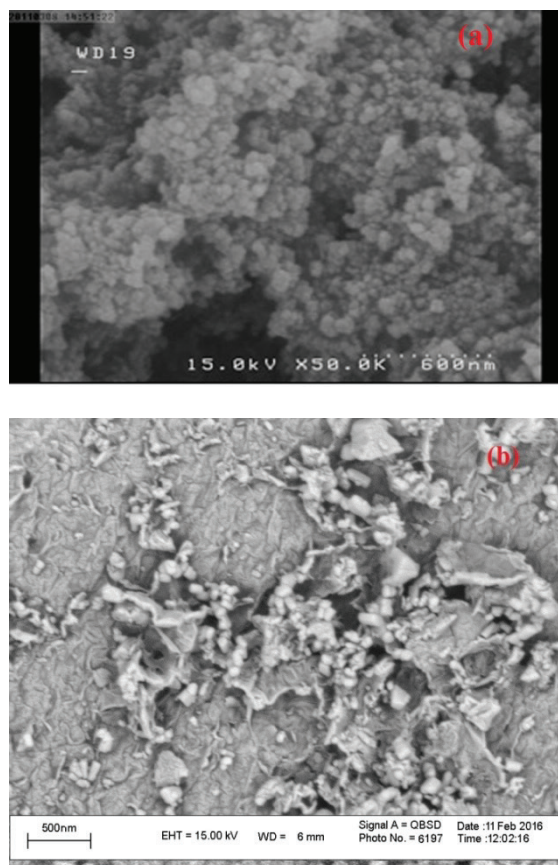


Fig. 3. The SEM of (a) $MgFe_2O_4$ and (b) $GO/MgFe_2O_4$.

Table 3
Analysis of variance (ANOVA) for the quadratic response surface model

Source of variations	Sum of squares	Degrees of freedom	Adjusted mean square	F Value
Regression	1,088.85	10	108.885	73.35
Residuals	29.69	20	1.484	
Total	1,118.54	30		

$$R^2 = 97.35\%, R^2_{\text{pred}} = 93.57\% \text{ and } R^2_{\text{adj}} = 96.02\%.$$

correlation criterion between the experimental data and the predicted responses. Fig. 4 shows a graph of the predicted response plotted by the model against the experimental responses. The determination coefficient (R^2) between the predicted values and the experimental values was 97.35%, indicating the validity of the model. This means that the experimental values are in good agreement with predicted values. This implies that 97.35% of the variations in arsenic removal efficiency is explained by the independent variables and this also means that the model does not explain only 2.65% of the variation. The predicted determination coefficient of the model (R^2_{pred}) was 0.9357, indicating that 93.57% of the response variation is attributed to the four independent factors. The adjusted R^2 (R^2_{adj}) = 0.9602 was also of statistical significance and indicates the correlation applicability of the model. The difference of R^2_{adj} and the R^2_{pred} value was less than 0.2 (20%), indicating the significance of the model.

In addition, the adequacy and the significance of the model were evaluated by the residuals which are the difference between experimental and the predicted response value. Normal probability plots are a suitable graphical method for judging the normality of the residuals. The normal probability plot in Fig. 5(a) shows the values of predicted response against the residual values, given by a normal distribution. A graph of the residual vs. the predicted response shows random behavior without a tendency toward residuals for experimental values Fig. 5(b). Fig. 5(c) shows the plot of residuals vs. order of data shows randomly scattering and consequently the residual plots approve the adequacy of the model.

On the other hand, the significance of the regression coefficient of the model terms was investigated by p value. In addition, the Student's t -test was used to determine the significance of the regression coefficient of the model terms, testing whether the true parameter is zero or not. p Value and t value of each term of the model are presented in Table 4.

Conventionally, the larger the t value and smaller the p value ($p < 0.05$) indicate the higher significance of the corresponding coefficient. The coefficients of the linear effect of time, arsenic concentration, adsorbent dosage and pH with p value < 0.05 were significant. In the case of quadratic effects of (X_i^2), the effects of X_2^2 , X_3^2 and X_4^2 were significant at the confidence level of 100%, and the term X_1^2 was removed from the model because of the high p value. In the case of binary terms, the interactions of X_1X_2 , X_1X_3 and X_3X_4 were significant at a confidence level of 100% and the other interactions were removed from the model because of the high p value.

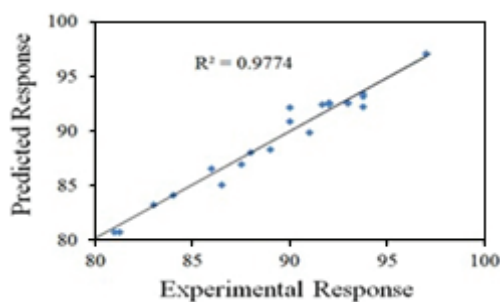


Fig. 4. Plot of the predicted and experimental values.

The Pareto analysis is a formal technique used to determine the relative importance of independent variables and each term of the model. Pareto analysis indicates the percentage effect of each term on the response, according to the following relation (Eq. (5)):

$$P_i = \left(\frac{b_i^2}{\sum b_i^2} \right) \times 100 (i \neq 0) \quad (5)$$

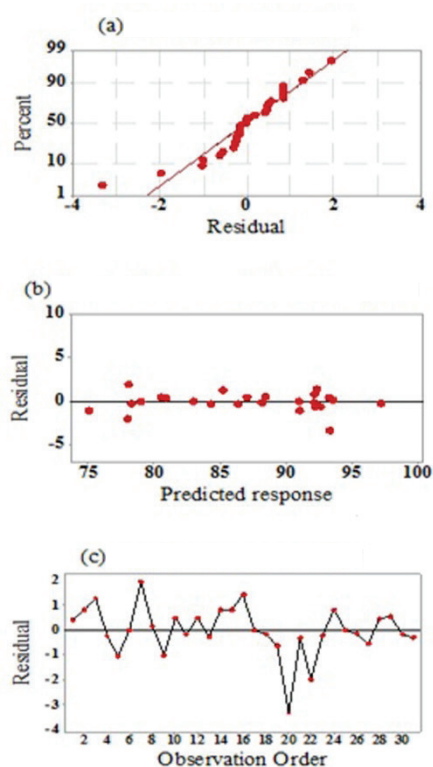


Fig. 5. Residual plots for predicted response by the model and experimental response. (a) Normal probability plot. (b) Residual plot vs. predicted response. (c) Residual plot vs. order.

Table 4
Estimated regression coefficient and corresponding t and p value

Term	Coefficient	t Value	p Value
Constant	92.172	231.95	0.000
X_1 (concentration)	0.583	2.35	0.029
X_2 (adsorbent dosage)	2.305	9.27	0.000
X_3 (time)	-1.375	-5.53	0.000
X_4 (pH)	-1.479	-5.95	0.000
X_2^2	-1.142	-5.04	0.000
X_3^2	-3.599	-15.89	0.000
X_4^2	-0.724	-3.20	0.005
X_1^2	-2.781	-9.13	0.000
X_1^2	-4.281	-14.06	0.000
X_3^2	-1.625	-5.34	0.000

The results of Pareto analysis are shown in Fig. 6. The results suggest that the $(X_1 * X_3)$ with the relative importance of 34.44% was the most important factor among the other factors in the removal of arsenic. The Pareto analysis suggested that order of relative importance of the four independent factors is as follows: adsorbent dosage > pH > contact time > arsenic concentration.

Among independent factors, the adsorbent dosage and pH are the most effective factors on the response. The Pareto analysis predicts that the arsenic concentration is not so impacted on the response rather to the independent factors. On the other hand, the following order was resulted in the relative importance of model terms: $X_1 * X_3$ (34.44%) > X_3^2 (24.34%) > $X_1 * X_2$ (14.53%) > X_2 (9.98%) > $X_3 * X_4$ (4.96%) > X_4 (4.11%) > X_3 (3.55%) > X_2^2 (2.45%) > X_4^2 (0.98%) > X_1 (0.63%).

The Minitab software provides a graphical route to study the interactions of the model terms by three-dimensional (3D) plots and 2D contours, which are suitable to study the binary interactions of factors.

Fig. 7 illustrates 3D surface plot and 2D contour for the combined interaction of adsorbent dosage and arsenic concentration on the adsorption capacity of arsenic. According to the figure, $X_1 X_2$ term has a negative effect on the response (adsorption capacity of arsenic) as evidenced by the negative terms in the model. The maximum effect on the response is observed at low of arsenic concentration and high level of adsorbent dosage meaning that the increasing the adsorbent dosage lead to increase the adsorption capacity. The statistical results are consistent with the literature and demonstrate the ability of the RSM at the prediction of the experimental results.

Fig. 8 illustrates 3D surface plot and 2D contour for the combined interaction of arsenic concentration and reaction time on the adsorption capacity of arsenic. According to this figure, the maximum degradation is at the arsenic concentration 50 ppm and reaction time 40 min.

Fig. 9 illustrates the 3D surface plot and 2D contour for the combined interaction of pH and reaction time on the adsorption capacity of arsenic. It is concluded that maximum degradation is at mid-levels of reaction time and minimum pH.

According to Eq. (4), the combined interaction of pH and contact time ($X_3 X_4$) has a negative impact on arsenic removal.

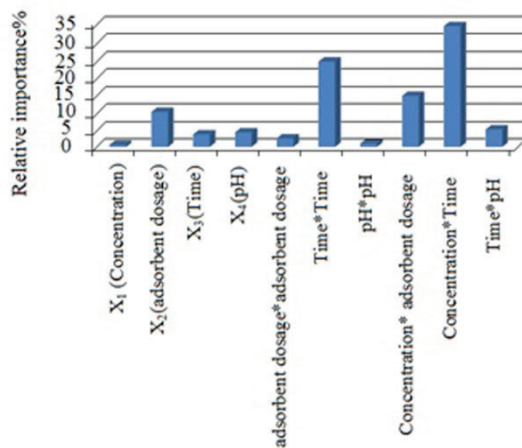


Fig. 6. Pareto chart analysis.

Hence, we expected the decrease of the arsenic removal percentage at higher pH. This could be explained by the pH_{pzc} of $MgFe_2O_4$. The pH_{pzc} of $MgFe_2O_4$ was determined to be 8.0–9.0.

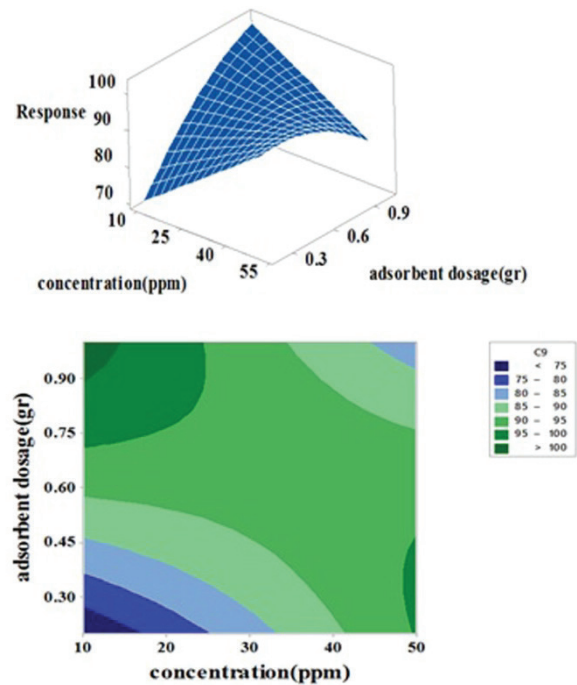


Fig. 7. The response surface plot and contour plot of the decolorization efficiency as the function of arsenic concentration and adsorbent dosage.

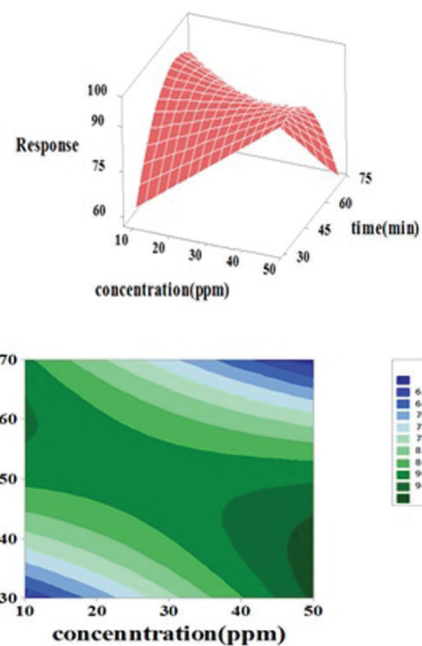


Fig. 8. The response surface plot and contour plot of the decolorization efficiency as the function of arsenic concentration and time.

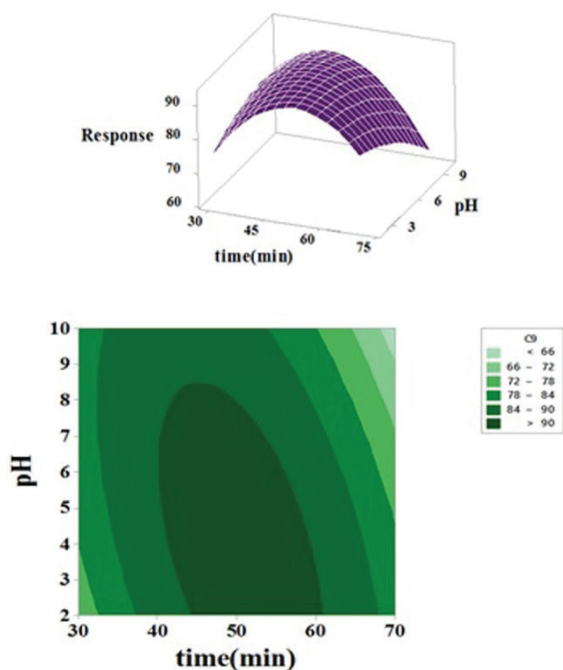


Fig. 9. The response surface plot and contour plot of the decolorization efficiency as the function of time and pH.

When pH is less than pH_{pzc} , the adsorbent surface is positively charged and arsenic is in the form of H_3AsO_3 , $\text{H}_2\text{AsO}_3^{2-}$ ($\text{pH} < 2.19$) and HAsO_3^{2-} ($\text{pH} = 6.94$). When pH higher than pH_{pzc} , the adsorbent ferrite surface is negatively charged and arsenic is mainly in the form of AsO_3^{3-} . Therefore, the increasing of electrostatic repulsion between the negative charges of adsorbent surface and negatively charge arsenite species result in to decrease the arsenic removal percentage at higher pH. In the case of $\text{GO}/\text{MgFe}_2\text{O}_4$, the pH_{pzc} was determined 7.8 and the similar behavior was observed in the acidic and basic medium.

Furthermore, the optimal conditions for the process of removal of arsenic by MgFe_2O_4 were predicted by the RSM. The optimum conditions of the adsorption process were predicted to be at pH, time, arsenic concentration and adsorbent dosage of 7.16, 30 min, 41 ppm and 0.03 g, respectively. The predicted response under these conditions was 99%, whereas the experimental test of predicted condition led to 97% removal of arsenic. Under optimum conditions, the capacity of MgFe_2O_4 for arsenic adsorption (Q_e) was 19.9 mg g^{-1} . At the same condition the removal percentage of arsenic by $\text{GO}/\text{MgFe}_2\text{O}_4$, GO was 95% and 92%, respectively.

4. Conclusion

MgFe_2O_4 adsorbent nanoparticles were successfully synthesized by the coprecipitation method and their performance at the removal of arsenic was investigated under the same conditions. To optimize the process and saving the cost and time of the study, the experiments were designed by central composite type of RSM through considering four process variables: initial arsenic concentration (ppm), adsorbent dosage (g), contact time (min) and pH. The optimum condition for the removal of arsenic was predicted by the RSM.

The predicted percentage removal of arsenic under optimum conditions was 99%, whereas the experimental testing of optimum condition led to 97% degradation for arsenic. The Pareto analysis predicted that the order of relative importance of the four independent factors is as follows: adsorbent dosage > pH > contact time > arsenic concentration. Under the identified optimum conditions, $\text{GO}/\text{MgFe}_2\text{O}_4$ nanocomposite exhibited better adsorption capacity than GO. The study revealed that MgFe_2O_4 could be a promising adsorbent for removal of industrial arsenic from aqueous solutions.

Acknowledgments

Special thanks to Iranian Nanotechnology Initiative Council and Urmia University for financial support.

References

- [1] A. Abbas, A.M. Al-Amer, T. Laoui, M.J. Al-Marri, M.S. Nasser, M. Khraisheh, M.A. Atieh, Heavy metal removal from aqueous solution by advanced carbon nanotubes: critical review of adsorption applications, *Sep. Purif. Technol.*, 157 (2016) 141–161.
- [2] M.M. Ali, M.L. Ali, M.S. Islam, M.Z. Rahman, Preliminary assessment of heavy metals in water and sediment of Karnaphuli River Bangladesh, *Environ. Nanotechnol. Monit. Manage.*, 5 (2016) 27–35.
- [3] X. Tang, H. Zheng, H. Teng, Y. Sun, J. Guo, W. Xie, Q. Yang, W. Chen, Chemical coagulation process for the removal of heavy metals from water: a review, *Desal. Wat. Treat.*, 57 (2016) 1733–1748.
- [4] Y. Huang, D. Wu, X. Wang, W. Huang, D. Lawless, X. Feng, Removal of heavy metals from water using polyvinyl amine by polymer-enhanced ultrafiltration and flocculation, *Sep. Purif. Technol.*, 158 (2016) 124–136.
- [5] V.K. Gupta, O. Moradi, I. Tyagi, S. Agarwal, H. Sadegh, R. Shahryari-Ghoshekandi, A.S.H. Makhlof, M. Goodarzi, A. Garshashi, Study on the removal of heavy metal ions from industry waste by carbon nanotubes: effect of the surface modification: a review, *Crit. Rev. Environ. Sci. Technol.*, 46 (2016) 93–118.
- [6] S. Huš, M. Kolar, P. Krajnc, Separation of heavy metals from water by functionalized glycidyl methacrylate poly (high internal phase emulsions), *J. Chromatogr., A*, 1437 (2016) 168–175.
- [7] E. Erdem, N. Karapinar, R. Donat, The removal of heavy metal cations by natural zeolites, *J. Colloid Interface Sci.*, 280 (2004) 309–314.
- [8] J. Qi, G. Zhang, H. Li, Efficient removal of arsenic from water using a granular adsorbent: Fe–Mn binary oxide impregnated chitosan bead, *Bioresour. Technol.*, 193 (2015) 243–249.
- [9] S. Lata, S.R. Samadder, Removal of arsenic from water using nano adsorbents and challenges: a review, *J. Environ. Manage.*, 166 (2016) 387–406.
- [10] B. Pan, Z. Li, Y. Zhang, J. Xu, L. Chen, H. Dong, W. Zhang, Acid and organic resistant nano-hydrated zirconium oxide (HZO)/ polystyrene hybrid adsorbent for arsenic removal from water, *Chem. Eng. J.*, 248 (2014) 290–296.
- [11] K.J. Reddy, K.J. Mc Donald, H. King, A novel arsenic removal process for water using cupric oxide nanoparticles, *J. Colloid Interface Sci.*, 397 (2013) 96–102.
- [12] M.S. Karmacharya, V.K. Gupta, I. Tyagi, S. Agarwal, V.K. Jha, Removal of As(III) and As(V) using rubber tire derived activated carbon modified with alumina composite, *J. Mol. Liq.*, 216 (2016) 836–844.
- [13] Y. Chen, C. Xiong, Adsorptive removal of As (III) ions from water using spent grain modified by polyacrylamide, *J. Environ. Sci.*, 45 (2016) 124–130.
- [14] Y. Chammui, P. Soosamiti, W. Naksata, S. Thiansem, O. Arqueropanyo, Removal of arsenic from aqueous solution by adsorption on Leonardite, *Chem. Eng. J.*, 240 (2014) 202–210.

- [15] A. Salimi, H. Mamkhezri, R. Hallaj, S. Soltanian, Electrochemical detection of trace amount of arsenic(III) at glassy carbon electrode modified with cobalt oxide nanoparticles, *Sens. Actuators, B*, 129 (2008) 246–254.
- [16] U. Shafique, A. Ijaz, M. Salman, W. Zaman, N. Jamil, R. Rehman, A. Javaid, Removal of arsenic from water using pine leaves, *J. Taiwan Inst. Chem. Eng.*, 43 (2012) 256–263.
- [17] S. Mandal, M.K. Sahu, R.K. Patel, Adsorption studies of arsenic(III) removal from water by zirconium polyacrylamide hybrid material (ZrPACM-43), *Water Resour. Ind.*, 4 (2013) 51–67.
- [18] V.M. Boddu, K. Abburi, J.L. Talbott, E.D. Smith, R. Haasch, Removal of arsenic (III) and arsenic (V) from aqueous medium using chitosan-coated biosorbent, *Water Res.*, 42 (2008) 633–642.
- [19] X. Luo, C. Wang, S. Luo, R. Dong, X. Tu, G. Zeng, Adsorption of As (III) and As (V) from water using magnetite Fe_3O_4 -reduced graphite oxide-MnO₂ nanocomposites, *Chem. Eng. J.*, 187 (2012) 45–52.
- [20] R. Rezaee, S. Nasser, A.H. Mahvi, R. Nabizadeh, S.A. Mousavi, A. Rashidi, A. Jafari, S. Nazmara, Fabrication and characterization of a polysulfone-graphene oxide nanocomposite membrane for arsenate rejection from water, *J. Environ. Health Sci. Eng.*, 13 (2015) 61–71.
- [21] R. Ebrahimi, A. Maleki, B. Shahmoradi, H. Daraei, A.H. Mahvi, A.H. Barati, A. Eslami, Elimination of arsenic contamination from water using chemically modified wheat straw, *Desal. Wat. Treat.*, 51 (2013) 2306–2316.
- [22] M.R. Boldaji, R. Nabizadeh, M.H. Dehghani, K. Nadafi, A.H. Mahvi, Evaluating the performance of iron nanoparticle resin in removing arsenate from water, *J. Environ. Sci. Health, Part A*, 45 (2010) 946–950.
- [23] E. Bazrafshan, H. Faridi, F.K. Mostafapour, A.H. Mahvi, Removal of arsenic from aqueous environments using *Moringa peregrina* seed extract as a natural coagulant, *Asian J. Chem.*, 25 (2013) 3557–3561.
- [24] T. Nurgaliev, Numerical investigation of the surface impedance of ferromagnetic manganite thin films, *J. Magn. Magn. Mater.*, 320 (2008) 304–311.
- [25] A. Sutka, G. Mezinskis, A. Pludons, S. Lagzdina, Characterization of sol-gel auto-combustion derived spinel ferrite nano-materials, *Power Eng.*, 56 (2010) 254–259.
- [26] H. Gao, C. Ma, B. Sun, Preparation and characterization of NiMn_2O_4 negative temperature coefficient ceramics by solid-state coordination reaction, *J. Mater. Sci. - Mater. Electron.*, 25 (2014) 3990–3995.
- [27] Z. Bazhan, F.E. Ghodsi, J. Mazloom, Surface morphology, optical, and electrochromic properties of nanostructured nickel ferrite (NiFe_2O_4) prepared by sol-gel method: effects of Ni/Fe molar ratios, *Appl. Phys. A*, 122 (2016) 551–561.
- [28] Q. Xu, Y. Wei, Y. Liu, X. Ji, L. Yang, M. Gu, Preparation of Mg/Fe spinel ferrite nanoparticles from Mg/Fe-LDH microcrystallites under mild conditions, *Solid State Sci.*, 11 (2009) 472–478.
- [29] C. Luadthong, V. Itthibenchapong, N. Viriya-empikul, K. Faungnawakij, P. Pavasant, W. Tanthapanichakoon, Synthesis, structural characterization, and magnetic property of nanostructured ferrite spinel oxides (AFe_2O_4 , A= Co, Ni and Zn), *Mater. Chem. Phys.*, 143 (2013) 203–208.
- [30] C. Yao, Q. Zeng, G.F. Goya, T. Torres, J. Liu, H. Wu, M. Ge, Y. Zeng, Y. Wang, J.Z. Jiang, ZnFe_2O_4 nanocrystals: synthesis and magnetic properties, *J. Phys. Chem. C*, 111 (2007) 12274–12278.
- [31] Z. Jia, Q. Qin, J. Liu, H. Shi, X. Zhang, R. Hu, S. Li, R. Zhu, The synthesis of hierarchical ZnFe_2O_4 architecture and their application for Cr(VI) adsorption removal from aqueous solution, *Superlattices Microstruct.*, 82 (2015) 174–187.
- [32] A. Pradeep, P. Priyadharsini, G. Chandrasekaran, Sol-gel route of synthesis of nanoparticles of MgFe_2O_4 and XRD, FTIR and VSM study, *J. Magn. Magn. Mater.*, 320 (2008) 2774–2779.
- [33] R. Köferstein, T. Walther, D. Hesse, S.G. Ebbinghaus, Preparation and characterization of nanosized magnesium ferrite powders by a starch-gel process and corresponding ceramics, *J. Mater. Sci.*, 48 (2013) 6509–6518.
- [34] H. Turkyilmaz, T. Kartal, S.Y. Yildiz, Optimization of lead adsorption of mordenite by response surface methodology: characterization and modification, *J. Environ. Health Sci. Eng.*, 12 (2014) 5–13.
- [35] J. Aravind, P. Kanmani, G. Sudha, R. Balan, Optimization of chromium(VI) biosorption using gooseberry seeds by response surface methodology, *Global J. Environ. Sci. Manage.*, 2 (2016) 61–68.
- [36] R. Voda, A. Negrea, L. Lupa, M. Ciopec, P. Negrea, C.M. Davidescu, M. Butnariu, Nanocrystalline ferrites used as adsorbent in the treatment process of waste waters resulted from ink jet cartridges manufacturing, *Open Chem.*, 13 (2015) 743–747.
- [37] V. Srivastava, Y. Sharma, M. Sillanpää, Application of nano-magneso ferrite ($n\text{-MgFe}_2\text{O}_4$) for the removal of Co^{2+} ions from synthetic wastewater: kinetic, equilibrium and thermodynamic studies, *Appl. Surf. Sci.*, 338 (2015) 42–54.
- [38] J. Hu, I. Lo, G. Chen, Comparative study of various magnetic nanoparticles for Cr(VI) removal, *Sep. Purif. Technol.*, 56 (2007) 249–256.
- [39] S.A. Hosseini, S. Mashaykhi, Sh. Babaei, Graphene oxide/zinc oxide nanocomposite: a superior adsorbent for removal of methylene blue-statistical analysis by response surface methodology (RSM), *S. Afr. J. Chem.*, 69 (2016) 105–112.